Electronic structure of $ThPd_2Al_3$: Impact of the U 5f states on the electronic structure of UPd_2Al_3

Shin-ichi Fujimori,[1] Yukiharu Takeda,[1] Hiroshi Yamagami,[1,2] Jiří Pospíšil,[3,4] Etsuji Yamamoto,[3] and Yoshinori Haga[3]

[1]*Materials Sciences Research Center, Japan Atomic Energy Agency, Sayo, Hyogo 679-5148, Japan*
[2]*Department of Physics, Faculty of Science, Kyoto Sangyo University, Kyoto 603-8555, Japan*
[3]*Advanced Science Research Center, Japan Atomic Energy Agency, Tokai, Ibaraki 319-1195, Japan*
[4]*Department of Condensed Matter Physics, Faculty of Mathematics and Physics, Charles University, Ke Karlovu 5, 121 16 Prague 2, Czech Republic*

(Received 1 December 2021; accepted 4 March 2022; published 22 March 2022)

The electronic structure of $ThPd_2Al_3$, which is isostructural to the heavy fermion superconductor UPd_2Al_3, was investigated by photoelectron spectroscopy. The band structure and Fermi surfaces of $ThPd_2Al_3$ were obtained by angle-resolved photoelectron spectroscopy (ARPES), and the results were well explained by the band-structure calculation based on the local density approximation. The comparison between the ARPES spectra and the band-structure calculation suggests that the Fermi surface of $ThPd_2Al_3$ mainly consists of the Al 3p and Th 6d states with a minor contribution from the Pd 4d states. The comparison of the band structures between $ThPd_2Al_3$ and UPd_2Al_3 argues that the U 5f states form Fermi surfaces in UPd_2Al_3 through hybridization with the Al 3p state in the Al layer, suggesting that the Fermi surface of UPd_2Al_3 has a strong three-dimensional nature.

DOI: 10.1103/PhysRevB.105.115128

I. INTRODUCTION

The coexistence of unconventional superconductivity and antiferromagnetic ordering with a relatively large magnetic moment ($0.85\mu_B$/U) is the most characteristic feature of the heavy fermion compound UPd_2Al_3 [1]. There are many electronic structure studies for UPd_2Al_3; however, the nature of the U 5f state in UPd_2Al_3 remains contradictory. The de Haas–van Alphen (dHvA) study reported that the observed dHvA branches are mostly explained by the band-structure calculation treating the U 5f states as being itinerant [2]. Its electronic structure has also been studied by photoelectron spectroscopy [3–7], and the itinerant nature of the U 5f states has been reported. A recent Compton scattering study has also reported that the U 5f states have an itinerant character at temperatures lower than $T = 20$ K [8], which is consistent with the angle-resolved photoelectron spectroscopy (ARPES) study [3]. Meanwhile, a resonant photoemission study on UPd_2Al_3 has also suggested the itinerant nature of the U 5f state, but there exists a correlated satellite structure due to the strong electron correlation effect [9]. In contrast, the transport properties of UPd_2Al_3 are very similar to those of heavy fermion Ce-based compounds, and they have been essentially understood based on the very localized U 5f picture. For example, the temperature dependence of the magnetic susceptibility has been interpreted based on the crystalline electric field scheme [10]. To understand these physical properties consistently, the dual model of the U 5f states has been proposed for this compound [11]. In this scenario, the U 5f states are formally divided into two subsystems: an itinerant f^1 component and a localized f^2 component. The result of the recent point contact spectroscopy study on UPd_2Al_3 was also interpreted along with this scenario [12], but the microscopic information of the U 5f states is still lacking. To understand the electronic structure of UPd_2Al_3, it is essential to identify the contribution of the U 5f state to gain a greater insight regarding its nature in this compound.

In the present paper, we have studied the electronic structure of $ThPd_2Al_3$, which is the f^0-reference compound of UPd_2Al_3, by photoelectron spectroscopy. We compared the ARPES spectra between $ThPd_2Al_3$ and UPd_2Al_3, and the contribution from the U 5f states to the band structure of UPd_2Al_3 was clarified. Furthermore, $ThPd_2Al_3$ is a superconductor with $T_C = 0.2$ K [13]. It is the only case where a uranium heavy fermion superconductor has an isostructural counterpart of the thorium compound, which is also a superconductor. Thus, $ThPd_2Al_3$ is in itself an important target material to study its electronic structure. We found that the band structure and the topology of the Fermi surface of $ThPd_2Al_3$ are essentially explained by the band-structure calculation based on the local density approximation.

II. EXPERIMENTAL PROCEDURE AND BAND-STRUCTURE CALCULATION

The $ThPd_2Al_3$ single crystal was grown by the Czochralski method at a pulling speed of 12 mm/h in a tetra-arc furnace under an Ar protective atmosphere. The final shape of the single crystal was a cylinder with a diameter of 2–3 mm and a length of 15 mm. The high quality of the single crystal was confirmed by the Laue method showing sharp spots and a residual resistance ratio RRR = 37 (the extrapolated value $\rho_0 = 0.7\ \mu\Omega$/cm) after 2 weeks annealing at 900 °C in an evacuated quartz ampule. Photoemission experiments were performed at the soft x-ray beamline BL23SU of SPring-8 [14]. The overall energy resolution in angle-integrated

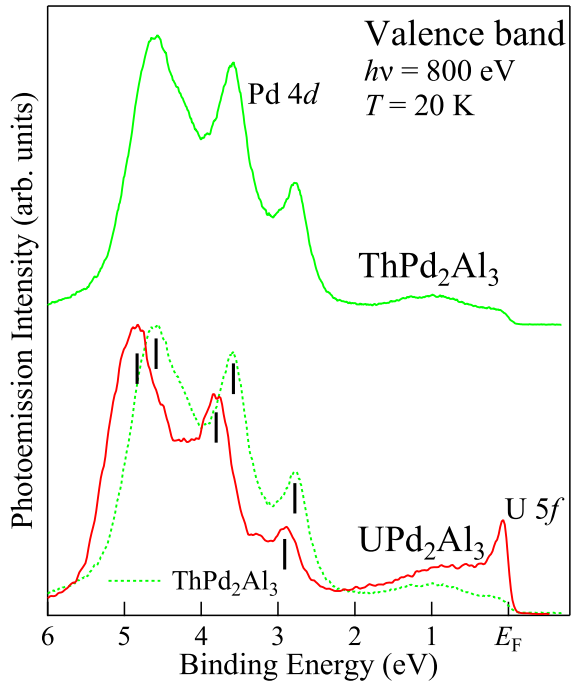

FIG. 1. Valence-band spectrum of $ThPd_2Al_3$ measured at $h\nu = 800$ eV. Also, the bottom part of this figure provides a comparison of the valence-band spectra of $ThPd_2Al_3$ and UPd_2Al_3 measured at $h\nu = 800$ eV.

photoemission (AIPES) experiments at $h\nu = 800$ eV was approximately 150 meV, and that in the ARPES experiments at $h\nu = 660$ eV was approximately 90 meV. Clean sample surfaces were obtained by cleaving the samples *in situ* perpendicular to the c axis under ultrahigh vacuum conditions. The vacuum during the course of measurements was typically $<2 \times 10^{-8}$ Pa, and the sample surfaces were stable for the entire duration of the measurements (about 2 days) since no significant changes had been observed in the ARPES spectra during these periods. The positions of the ARPES cuts in the momentum space were determined by assuming a free-electron final state with an inner potential of $V_0 = 12$ eV.

In the band-structure calculations, relativistic linear augmented plane-wave (RLAPW) calculations [15] within the local density approximation (LDA) [16] were performed, treating all U $5f$ electrons as itinerant. In this approach, the Dirac-type Kohn-Sham equation has been formulated, and the spin-orbit interaction is exactly taken into account [17]. To compare the results of the calculation with the ARPES spectra, we have simulated the ARPES spectral functions on the basis of the band-structure calculation. In the simulation, the following effects were taken into account: (i) the broadening along the $k_\perp$ direction due to the finite escape depth of the photoelectrons, (ii) the lifetime broadening of the photohole, (iii) the photoemission cross sections of orbitals, and (iv) the energy resolution and the angular resolution of the electron analyzer. The details are outlined in Ref. [18].

III. RESULTS AND DISCUSSION

Figure 1 shows the AIPES valence-band spectrum of $ThPd_2Al_3$ measured at $h\nu = 800$ eV and its comparison with that of UPd_2Al_3. According to the photoionization cross sections, the contributions from the Pd $4d$ and U $5f$ states are dominant in this photon energy [19], and thus three prominent peaks located between $E_B = 2.5$ and 6 eV are ascribed to the contributions from the Pd $4d$ states. The bottom part of this figure demonstrates the comparison between the valence-band spectra of $ThPd_2Al_3$ and UPd_2Al_3 measured at $h\nu = 800$ eV. The comparison shows that the sharp peak at the Fermi energy exists only in the spectrum of UPd_2Al_3, suggesting that the peak found at the Fermi energy represents the contribution of the U $5f$ states in UPd_2Al_3. This is consistent with the result of the resonant photoemission experiment for UPd_2Al_3 in which a similar similar sharp peak was observed at the Fermi energy of UPd_2Al_3 [9]. A further important point to note is that all three Pd $4d$ peaks in the valence-band spectrum of UPd_2Al_3 are located in higher binding energies than those in the valence-band spectrum of $ThPd_2Al_3$. A very similar rigid shift of the transition metal d bands has been observed in the valence-band spectra of URu_2Si_2 and $ThRu_2Si_2$ [20]. The amount of energy shift is approximately 200 meV, which is also very similar to the case between $ThRu_2Si_2$ and URu_2Si_2. This energy shift of the d band is in contrast with the case of the U $5f$ localized compound UPd_3 where no shift was observed in the Pd $4d$ bands between $ThPd_3$ and UPd_3 [21]. The rigid shift in the Pd $4d$ states between UPd_2Al_3 and $ThPd_2Al_3$ suggests that the U $5f$ states are involved in the valence-band structure of UPd_2Al_3, and they are not impuritylike contributions as expected when the U $5f$ states are almost localized. Next, we discuss the band structure and Fermi surface of $ThPd_2Al_3$ measured by ARPES. Figure 2 summarizes the result of the ARPES study of $ThPd_2Al_3$. Figure 2(a) shows the ARPES spectra of $ThPd_2Al_3$ along the K-M-K-Γ-M-Γ high-symmetry line measured at $h\nu = 660$ eV. The spectra consist of two different types of energy dispersions, namely very dispersive bands at $E_F \lesssim E_B \lesssim 2.5$ eV and less dispersive bands with enhanced intensities distributed at $E_B \gtrsim 2.5$ eV. Since the photoionization cross section of the Pd $4d$ states is more than 30 times enhanced than those of Al $3s$, $3p$ and Th $6d$ states [19], the prominent dispersions at $E_B \gtrsim 2.5$ eV are the contributions from the Pd $4d$ states. Furthermore, the dispersive bands at $E_F \lesssim E_B \lesssim 2.5$ eV reflect the contributions mainly from the Al and Th states.

Figure 2(b) shows the calculated band structure and the simulation of the ARPES spectra based on the band-structure calculation. The solid lines and the density plot represent the calculated energy dispersions and the simulation, respectively. The color coding of each band represents the contribution from the Pd $4d$ states. The experimental band structure is well explained by the band-structure calculation. For example, the parabolic dispersions centered at the Γ point that forms the Fermi surface are in good agreement with the calculated bands 16-18. There are also parabolic dispersions along the K-M-K high-symmetry line, which are also well explained by the calculated band 15. At higher binding energies, the nearly flat Pd $4d$ bands in the experimental ARPES spectra agree with the bands 2–13 in the calculation. Although the Pd $4d$ bands are not clearly resolved one by one in the experimental spectra, the overall features agree very well between experimental ARPES spectra and the calculated band structure. Note that the contribution from the Pd $4d$ states is distributed in

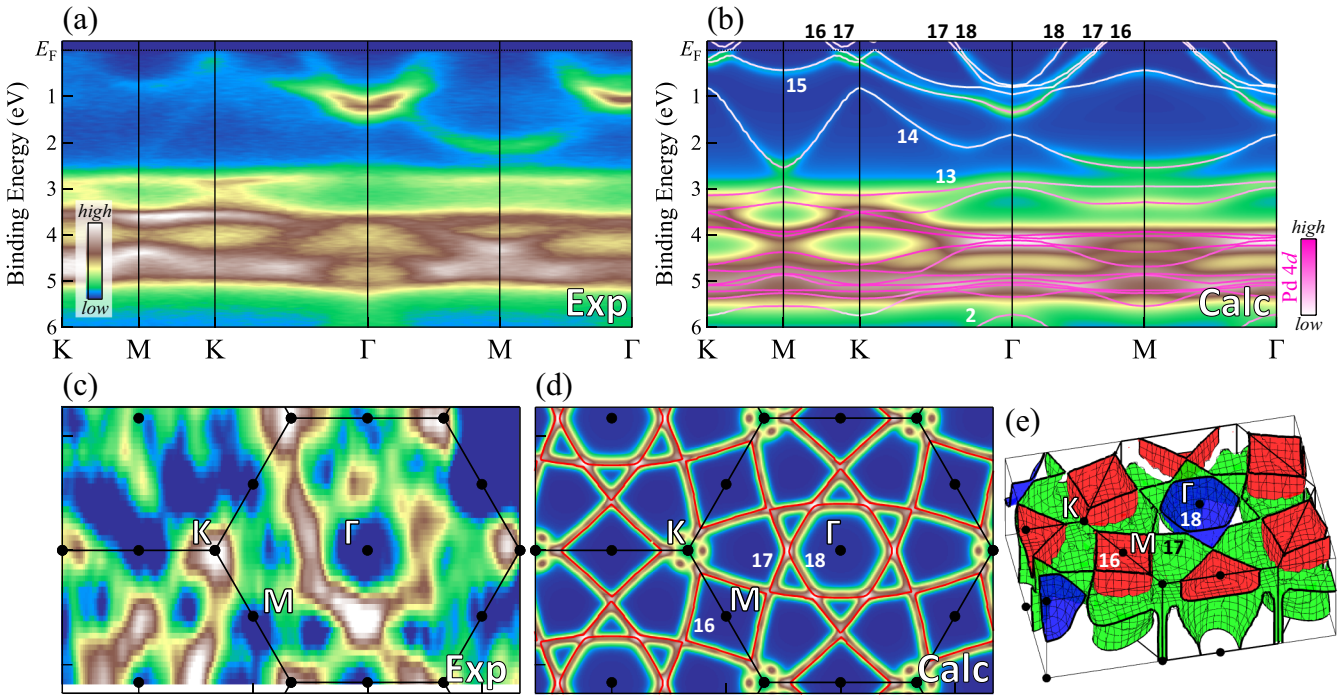

FIG. 2. Band structure and Fermi surface of $ThPd_2Al_3$ obtained by ARPES. (a) ARPES spectra of $ThPd_2Al_3$ measured along the K-M-K-Γ-M-Γ high-symmetry line at $h\nu = 660$ eV. (b) Calculated band structure and simulation of the ARPES spectra based on the band-structure calculation. (c) Fermi-surface map obtained by the integration of the ARPES spectra over 100 meV across E_F. (d) Calculated Fermi surface and the simulation of the experimental Fermi-surface map. (e) Three-dimensional shape of the calculated Fermi surfaces.

higher binding energies ($E_B \gtrsim 2.5$ eV), and the Fermi surface of $ThPd_2Al_3$ mainly consists of the Al and Th states. This situation is significantly different from the case of $ThRu_2Si_2$ where the transition metal d band is close to the Fermi energy, and the d bands are hybridized with the U $5f$ states in URu_2Si_2 [20,22]. We further discuss the orbital character of the Fermi surface of $ThPd_2Al_3$ and UPd_2Al_3 in the latter part of this section.

Figure 2(c) shows the experimental Fermi-surface map of $ThPd_2Al_3$, which was obtained by integrating the photoemission intensity over 100 meV across E_F. There is a hexagonal-shaped feature with enhanced intensity centered at the Γ point. In addition, the intensity at the K point is also enhanced and these points are connected to each other and form a very complex shape. In Fig. 2(d), we illustrate the calculated Fermi surface using solid curves, and we also demonstrate the simulation of the Fermi-surface map based on the band-structure calculation as a density plot. The three-dimensional shape of the calculated Fermi surfaces of $ThPd_2Al_3$ is also shown in Fig. 2(e). In the band-structure calculation, the bands 16–18 form Fermi surfaces. Bands 16 and 18 form a hole-type Fermi surface around the M point and an electron-type Fermi surface around the Γ point, respectively. In contrast, band 17 forms a very complicated Fermi surface with a three-dimensional shape, but forms the electron-type Fermi surface with a starlike shape around the Γ point. Experimental and calculated Fermi surfaces agree very well although the features are broader in the experimental map compared to the calculated map. Despite the fact that the details of the experimental Fermi surface are not very clear, the topology of the Fermi surface agrees with the result of the band-structure calculation. Accordingly, the band structure and Fermi surface of $ThPd_2Al_3$ were well explained by the band-structure calculation.

Next, we performed a comparison between the ARPES spectra of $ThPd_2Al_3$ and UPd_2Al_3 to reveal the contribution of the U $5f$ states in the band structure of UPd_2Al_3, as shown in Fig. 3. Figures 3(a) and 3(b) represent the experimental ARPES spectra of $ThPd_2Al_3$ and the corresponding calculated band structure, respectively. The color coding of the calculated bands corresponds to the contributions from the Th $6d$ and the Al $3p$ states. Note that the contribution from the Al $3s$ is almost negligible in these binding energies. The experimental ARPES spectra are well explained by the band-structure calculation, as discussed in Figs. 2, and thus the orbital character of each band should also agree with the result of the band-structure calculation. The calculation suggests that the Fermi surface of $ThPd_2Al_3$ mainly consists of the Al $3p$ and Th $6d$ states, but it has an enhanced Al $3p$ character. In particular, bands 17 and 18, which form the Fermi surfaces, have a dominant contribution from the Al $3p$ states, and the overall good agreement between the experimental data and the respective calculations suggests that the Fermi surfaces should have an enhanced contribution from the Al $3p$ states.

Figures 3(c) and 3(d) show the experimental ARPES spectra of UPd_2Al_3 and the corresponding calculated band structure. The ARPES spectra of UPd_2Al_3 were taken from Ref. [7]. The U $5f$ difference spectrum obtained by a resonant photoemission measurement [9] and the calculated U $5f$ density of states (DOS) are shown in the right panel of Fig. 3(c). The ARPES spectra were recorded at $h\nu = 600$ eV, and the

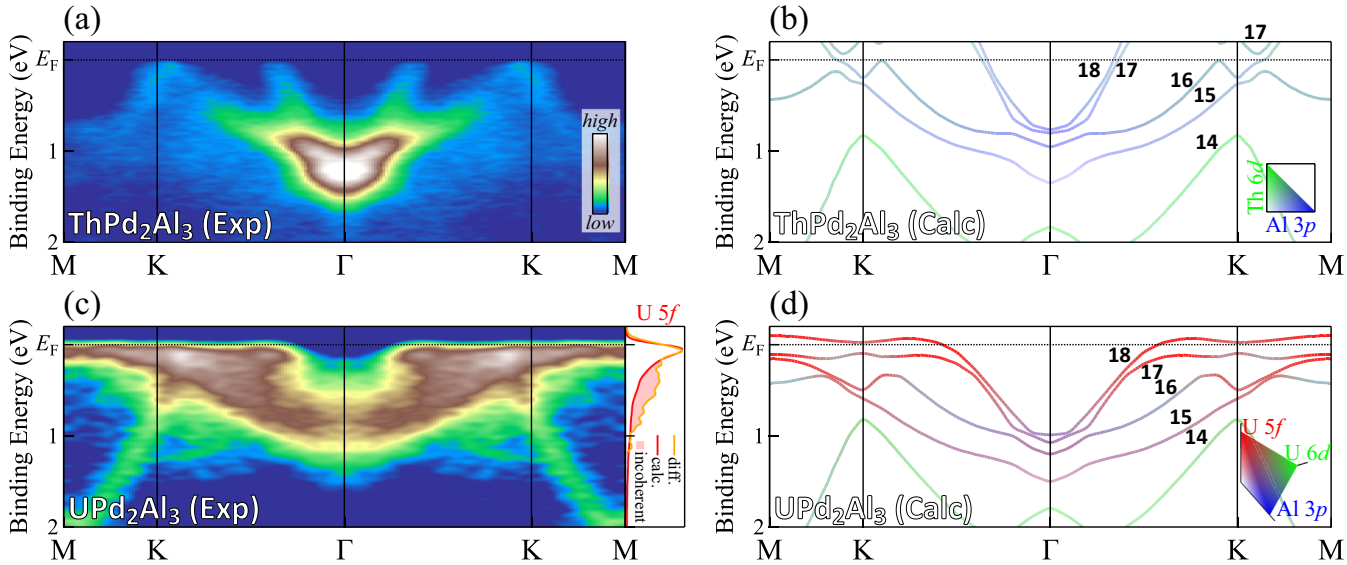

FIG. 3. Comparison between the ARPES spectra of $ThPd_2Al_3$ and UPd_2Al_3, and the result of the band-structure calculations. (a) ARPES spectra of $ThPd_2Al_3$ measured along the Γ-*K*-*M* high-symmetry line at $h\nu = 660$ eV. (b) Result of the band-structure calculation for $ThPd_2Al_3$. The color coding of each band represents the contributions from the Th 6*d* and the Al 3*p* states. (c) ARPES spectra of UPd_2Al_3 measured along the Γ-*K*-*M* high-symmetry line at $h\nu = 600$ eV. Data adapted from Ref. [7]. The U 5*f* difference spectrum obtained by resonant photoemission measurement [9] and the calculated U 5*f* DOS are shown in the right panel. (d) Result of the band-structure calculation for UPd_2Al_3. The color coding of each band represents the contributions from the U 5*f*, U 6*d*, and the Al 3*p* states.

sample temperature was 20 K. The experimental energy dispersions of $ThPd_2Al_3$ and UPd_2Al_3 are very similar to each other, but the intensity of the energy dispersions distributed at $E_B = E_F - 1.2$ eV is enhanced in the spectra of UPd_2Al_3. Moreover, there exist very flat features in the vicinity of E_F, which represent the contributions from the U 5*f* states since the photoionization cross section of the U 5*f* states is dominant at the used photon energy. The overall structures of the experimental spectra of UPd_2Al_3 are also essentially explained by the band-structure calculation although the detail of each dispersion was not resolved experimentally. In particular, the very flat features at E_F originate from the renormalized U 5*f* bands due to the strong electron correlation effect.

The comparison between the ARPES spectra of $ThPd_2Al_3$ and UPd_2Al_3 indicates that the U 5*f* states are strongly hybridized with the non-*f* dispersive bands in $ThPd_2Al_3$ which correspond to the calculated bands 15–18 of $ThPd_2Al_3$. These calculated bands have an enhanced contribution from the Al 3*p* states, suggesting that the U 5*f* states are strongly hybridized with the Al 3*p* states in UPd_2Al_3. The crystal structure of UPd_2Al_3 consists of alternating stacks of U-Pd and Al layers along the *c* axis, and the presence of the enhanced U 5*f*-Al 3*p* hybridization suggests that the U 5*f* states have a strong three-dimensional nature similar to the case of the heavy fermion compound URu_2Si_2 [22]. As a result, the Fermi surface of UPd_2Al_3 should also have a strong three-dimensional nature due to the enhanced U 5*f*-Al 3*p* hybridization. Previous ARPES studies of UPd_2Al_3 [4,6] have shown a cylindrical Fermi surface along the Γ- *A* line. The Fermi surface has an enhanced contribution from the U 5*f* states, but the present result suggests that it also has an enhanced contribution from the Al 3*p* states.

Note that the U 5*f* states have a strong electron correlation effect, and the U 5*f* states in UPd_2Al_3 have an incoherent peak distributed at approximately $E_B = 0.2$–1 eV [9]. Thus, the experimental bands around this binding energy should have the contribution from the incoherent component of the U 5*f* states. This is consistent with the dual nature of the U 5*f* states in UPd_2Al_3 as proposed theoretically, where the heavy quasiparticle band is described by the effective renormalized theory while the high-energy structure is explained by the multiplet sidebands arising from the Hund's rule [23,24]. Experimentally, there are no nondispersive but dispersive bands in this binding energy region, and thus the energy dispersions in $E_B = 0.2$–1 eV are hybridized with the incoherent U 5*f* states. It is theoretically proposed that the localized multiplet bands are hybridized with dispersive bands with non-*f* character [24], and the experimental spectra are consistent with the theory.

IV. CONCLUSION

In the present study, we investigated the electronic structure of $ThPd_2Al_3$ using photoelectron spectroscopy, and the results were compared with the band-structure calculation and the spectra of the isostructural heavy fermion superconductor UPd_2Al_3. The Pd 4*d* states in the valence-band spectrum of $ThPd_2Al_3$ were found to be shallower than those in the valence-band spectrum of UPd_2Al_3 by approximately 200 meV, suggesting that the U 5*f* states are involved in the valence-band structure of UPd_2Al_3, and are not impurity-like contributions. The Fermi surface and the band structure of $ThPd_2Al_3$ obtained by ARPES were well explained by the band-structure calculation. The electronic structure in the very vicinity of E_F is dominated by contributions

from the Al $3p$ and Th $6d$ states with minor contributions from the Pd $4d$ states. The comparison between the ARPES spectra of $ThPd_2Al_3$ and UPd_2Al_3 suggests that the electronic structure of UPd_2Al_3 in the very vicinity of E_F is dominated by the enhanced U $5f$-Al $3p$ hybridization. This indicates that the electronic structure of UPd_2Al_3 has a three-dimensional nature [25–31].

ACKNOWLEDGMENTS

The experiment was performed under Proposal No. 2015B3820 at SPring-8 BL23SU. The present work was financially supported by JSPS KAKENHI Grants No. JP26400374, No. JP16H01084, No. JP18K03553, and No. JP20KK0061.

[1] C. Geibel, C. Schank, S. Thies, H. Kitazawa, C. Bredl, A. Bohm, M. Rau, A. Grauel, R. Caspary, R. Helfrich, U. Ahlheim, G. Weber, and F. Steglich, Heavy-fermion superconductivity at $T_c = 2$ K in the antiferromagnet UPd_2Al_3, Z. Phys. B **84**, 1 (1991).

[2] Y. Inada, H. Yamagami, Y. Haga, K. Sakurai, Y. Tokiwa, T. Honma, E. Yamamoto, Y. Ōnuki, and T. Yanagisawa, Fermi Surface and de Haas-van Alphen oscillation in both the normal and superconducting mixed states of UPd_2Al_3, J. Phys. Soc. Jpn. **68**, 3643 (1999).

[3] S. Fujimori, Y. Saitoh, T. Okane, A. Fujimori, H. Yamagami, Y. Haga, E. Yamamoto, and Y. Ōnuki, Itinerant to localized transition of f electrons in the antiferromagnetic superconductor UPd_2Al_3, Nat. Phys. **3**, 618 (2007).

[4] S. Fujimori, T. Ohkochi, T. Okane, Y. Saitoh, A. Fujimori, H. Yamagami, Y. Haga, E. Yamamoto, and Y. Onuki, Angle resolved photoemission study on uranium compounds, IOP Conf. Ser.: Mater. Sci. Eng. **9**, 012045 (2010).

[5] S. Fujimori, T. Ohkochi, I. Kawasaki, A. Yasui, Y. Takeda, T. Okane, Y. Saitoh, A. Fujimori, H. Yamagami, Y. Haga, E. Yamamoto, Y. Tokiwa, S. Ikeda, T. Sugai, H. Ohkuni, N. Kimura, and Y. Ōnuki, Electronic structure of heavy fermion uranium compounds studied by core-level photoelectron spectroscopy, J. Phys. Soc. Jpn. **81**, 014703 (2012).

[6] S. Fujimori, I. Kawasaki, A. Yasui, Y. Takeda, T. Okane, Y. Saitoh, A. Fujimori, H. Yamagami, Y. Haga, E. Yamamoto, and Y. Ōnuki, Angle resolved photoelectron spectroscopy study of heavy fermion superconductor UPd_2Al_3, JPS Conf. Proc. **3**, 011072 (2014).

[7] S. Fujimori, Y. Takeda, T. Okane, Y. Saitoh, A. Fujimori, H. Yamagami, Y. Haga, E. Yamamoto, and Y. Ōnuki, Electronic structures of uranium compounds studied by soft x-ray photoelectron spectroscopy, J. Phys. Soc. Jpn. **85**, 062001 (2016).

[8] A. Koizumi, Y. Kubo, E. Yamamoto, Y. Haga, and Y. Sakurai, Electronic structure in heavy fermion compound UPd_2Al_3 through directional Compton profile measurement, J. Phys. Soc. Jpn. **88**, 034714 (2019).

[9] S. I. Fujimori, M. Kobata, Y. Takeda, T. Okane, Y. Saitoh, A. Fujimori, H. Yamagami, Y. Haga, E. Yamamoto, and Y. Ōnuki, Manifestation of electron correlation effect in $5f$ states of uranium compounds revealed by $4d$-$5f$ resonant photoelectron spectroscopy, Phys. Rev. B **99**, 035109 (2019).

[10] A. Grauel, A. Böhm, H. Fischer, C. Geibel, R. Köhler, R. Modler, C. Schank, F. Steglich, G. Weber, T. Komatsubara, and N. Sato, Tetravalency and magnetic phase diagram in the heavy-fermion superconductor UPd_2Al_3, Phys. Rev. B **46**, 5818 (1992).

[11] G. Zwicknagl, A. Yaresko, and P. Fulde, Fermi surface and heavy masses for UPd_2Al_3, Phys. Rev. B **68**, 052508 (2003).

[12] N. K. Jaggi, O. Mehio, M. Dwyer, L. H. Greene, R. E. Baumbach, P. H. Tobash, E. D. Bauer, J. D. Thompson, and W. K. Park, Hybridization gap in the heavy-fermion compound UPd_2Al_3 via quasiparticle scattering spectroscopy, Phys. Rev. B **95**, 165123 (2017).

[13] M. Maple, M. de Andrade, J. Herrmann, Y. Dalichaouch, D. Gajewski, C. Seaman, R. Chau, R. Movshovich, M. Aronson, and R. Osborn, Non Fermi liquid ground states in strongly correlated f-electron materials, J. Low Temp. Phys. **99**, 223 (1995).

[14] Y. Saitoh, Y. Fukuda, Y. Takeda, H. Yamagami, S. Takahashi, Y. Asano, T. Hara, K. Shirasawa, M. Takeuchi, T. Tanaka, and H. Kitamura, Performance upgrade in the JAEA actinide science beamline BL23SU at SPring-8 with a new twin-helical undulator, J. Synchrotron Rad. **19**, 388 (2012).

[15] H. Yamagami, All-electron spin-polarized relativistic linearized APW method: Electronic and magnetic properties of BCC Fe, HCP Gd and uranium monochalcogenides, J. Phys. Soc. Jpn. **67**, 3176 (1998).

[16] U. von Barth and L. Hedin, A local exchange-correlation potential for the spin polarized case. I, J. Phys. C: Solid State Phys. **5**, 1629 (1972).

[17] See Supplemental Material at http://link.aps.org/supplemental/10.1103/PhysRevB.105.115128 for detailed information.

[18] S. I. Fujimori, T. Ohkochi, T. Okane, Y. Saitoh, A. Fujimori, H. Yamagami, Y. Haga, E. Yamamoto, and Y. Ōnuki, Itinerant nature of U $5f$ states in uranium mononitride revealed by angle-resolved photoelectron spectroscopy, Phys. Rev. B **86**, 235108 (2012).

[19] J. Yeh and I. Lindau, Atomic subshell photoionization cross sections and asymmetry parameters: $1 \leqslant Z \leqslant 103$, At. Data Nucl. Data Tables **32**, 1 (1985).

[20] S. I. Fujimori, M. Kobata, Y. Takeda, T. Okane, Y. Saitoh, A. Fujimori, H. Yamagami, Y. Matsumoto, E. Yamamoto, N. Tateiwa, and Y. Haga, Electronic structure of $ThRu_2Si_2$ studied by angle-resolved photoelectron spectroscopy: Elucidating the contribution of U $5f$ states in URu_2Si_2, Phys. Rev. B **96**, 125117 (2017).

[21] T. Nautiyal, S. Auluck, P. Blaha, and C. Ambrosch-Draxl, Electronic structure and optical properties of $ThPd_3$ and UPd_3, Phys. Rev. B **62**, 15547 (2000).

[22] S. Fujimori, Y. Takeda, H. Yamagami, E. Yamamoto, and Y. Haga, Electronic structure of URu_2Si_2 in paramagnetic phase: three-dimensional angle resolved photoelectron spectroscopy study, Electron. Struct. **3**, 024008 (2021).

[23] G. Zwicknagl and M. Reese, Dual nature of strongly correlated $5f$ electrons, J. Magn. Magn. Mater. **310**, 201 (2007).

[24] G. Zwicknagl, $5f$ electrons in actinides: Dual nature and photoemission spectra, in *Condensed Matter Theories*, edited by H. Reinholz, G. Röpke, and M. de Llano (World Scientific, Singapore, 2007), Vol. 22, pp. 194–205.

[25] D. J. Singh and J. Nordström, *Planewaves, Pseudopotentials and the LAPW Method*, 2nd ed. (Springer, Berlin, 2006).

[26] H. Yamagami and Y. Kitawaki, Spin-polarized relativistic calculations in linear augmented-Slater-type-orbital method, Electron. Struct. **3**, 034003 (2021).

[27] J. J. Sakurai, *Advanced Quantum Mechanics* (Addison-Wesley, Boston, 1967).

[28] T. L. Loucks, *Augmented Plane Wave Method: A Guide to Performing Electronic Structure Calculations* (W. A. Benjamin, New York, 1967).

[29] O. K. Andersen, Linear methods in band theory, Phys. Rev. B **12**, 3060 (1975).

[30] H. Yamagami, A. Mavromaras, and J. Kübler, Magnetic properties of f-electron systems in spin-polarized relativistic density functional theory, J. Phys.: Condens. Matter **9**, 10881 (1997).

[31] P. E. Blöckl, O. Jepson, and O. K. Anderson, Improved tetrahedron method for Brillouin-zone integrations, Phys. Rev. B **49**, 16223 (1994).